Spectroscopic Signatures of Fractionalization in Octupolar Quantum Spin Ice

Félix Desrochers[*] and Yong Baek Kim[†]

Department of Physics, University of Toronto, Toronto, Ontario M5S 1A7, Canada

Recent investigations on the dipolar-octupolar compounds $Ce_2Zr_2O_7$ and $Ce_2Sn_2O_7$ suggest that they may stabilize so-called π-flux octupolar quantum spin ice (π-O-QSI), a novel three-dimensional quantum spin liquid hosting emergent photons. Confirmation of such an exotic phase would require the prediction of a distinctive signature and its subsequent experimental observation. So far, however, theoretical predictions for any such sharp smoking-gun signatures are lacking. In this Letter, we thoroughly investigate O-QSI using an extension of gauge mean-field theory. This framework produces a phase diagram consistent with previous work and an energy-integrated neutron scattering signal with intensity-modulated rod motifs, as reported in experiments and numerical studies. We predict that the dynamical spin structure factor of π-O-QSI is characterized by a broad continuum with three distinctive peaks as a consequence of the two mostly flat spinon bands. These three peaks should be measurable by high-resolution inelastic neutron scattering. Such spectroscopic signatures would be clear evidence for the realization of π-flux quantum spin ice.

Introduction.—Quantum spin liquids (QSLs) are quantum paramagnetic ground states of spin systems where competition between local interactions prevents conventional long-range order (LRO) and instead results in a long-range entangled (LRE) state supporting fractionalized excitations coupled to emergent gauge fields [1–8]. Decades after their initial proposal, the quest for an unequivocal experimental realization of a QSL remains a current endeavor—a testimony to how formidable of a task identifying a QSL is. Indeed, even though the experimental observation of fractionalized quasiparticles or emergent gauge fields would be direct evidence for a QSL ground state, conventional probes do not usually offer such unambiguous detection. For instance, a widely used method to "diagnose" a QSL is through the lack of signatures indicating LRO and the presence of a broad continuum in inelastic neutron scattering. However, this is an unconvincing state of affairs considering that scattering continua can be indicative of much less exotic phenomena than a continuum of fractionalized quasiparticles [9–14]. Therefore, since the universal features of QSLs (i.e., LRE) are not easily reachable by currently available probes, one has to resort to a much more careful and systematic approach where the microscopic parameters of a candidate material are first estimated by fitting a plethora of experimental measurements (e.g., heat capacity, magnetization, neutron scattering). Specific predictions about the nature of the ground state and its distinctive signatures can then be made to be later confirmed by empirical studies.

Recent investigations on the dipolar-octupolar (DO) compounds $Ce_2Zr_2O_7$ [15–22], $Ce_2Sn_2O_7$ [23,24], and $Ce_2Hf_2O_7$ [25,26] have been particularly exciting in that regard. A large amount of experimental evidence indicates that they may be a realization of quantum spin ice (QSI); a QSL with an emergent compact $U(1)$ gauge structure that provides a lattice realization of quantum electrodynamics [27–31]. In these DO compounds, the lowest lying doublet of the magnetically active ions forming a pyrochlore lattice can be described by pseudospin-1/2 with two components (S^x, S^z) that transform as dipoles and one (S^y) as an octupolar moment [32,33]. The most general Hamiltonian with nearest-neighbor couplings can be written as an XYZ model in a rotated local basis $\mathcal{H} = \sum_{\langle i,j \rangle} [J_{xx}S_i^x S_j^x + J_{yy}S_i^y S_j^y + J_{zz}S_i^z S_j^z]$.

Combinations of experimental measurements and theoretical analyses have now strongly constrained the microscopic exchange parameters for $Ce_2Zr_2O_7$, $Ce_2Hf_2O_7$, and $Ce_2Sn_2O_7$. They indicate that the leading coupling is most likely associated with the octupolar component (i.e., $|J_{yy}| > |J_{xx}|, |J_{zz}|$) [18,19,24,26], and in a region of parameter space that is predicted to realize the so-called π-flux octupolar quantum spin ice (π-O-QSI) phase, although conflicting results on $Ce_2Sn_2O_7$ have recently been reported [34]. In the π-O-QSI phase, the hexagonal plaquettes of the pyrochlore lattice are threaded by a static π flux of the emergent gauge field [see Figs. 1(a) and 1(b)] [35–41].

Even if the position of these compounds is solidly established in parameter space, there are still doubts regarding the nature of their ground state. The experimentally identified parameters are far from the perturbative Ising limit where the theoretical prediction for the π-flux QSI ground state is well established and disorder or
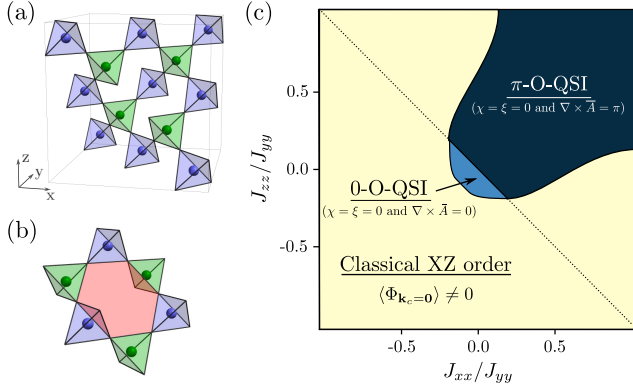
FIG. 1. (a) The network of corner-sharing tetrahedra forming the pyrochlore lattice and the sites of its parent (premedial) diamond lattice. (b) Hexagonal plaquettes of the pyrochlore lattice. (c) GMFT phase diagram of DO systems in the octupolar dominant regime. The dotted line indicates the $J_\pm = 0$ boundary.

interactions beyond the *XYZ* model could potentially stabilize other competing states [21]. These suspicions would be put aside if a prediction for a specific and distinct signature of the π-flux state could be experimentally observed. So far, no theoretical study of octupolar quantum spin ice (O-QSI) has been able to put forward such experimentally accessible smoking-gun signatures.

In this Letter, we present a comprehensive study of O-QSI using a recently introduced extension of gauge mean field theory (GMFT) [42]. We first classify all symmetric GMFT *Ansätze* and study their stability to produce a phase diagram widely consistent with previous numerical investigations [43–47]. We then compute the equal-time and dynamical spin structure factor for the 0- and π-flux O-QSI states. It is crucially highlighted that, due to their two largely flat energy bands, the spinons' contribution to the dynamical spin structure factor of the π-flux state is formed of a broad continuum with three distinctive peaks, in contrast to only one peak in the 0-flux phase. This highly distinctive and unique feature should be accessible by neutron scattering on either powder or single crystal samples with a resolution of about an order of magnitude higher than the leading exchange coupling J_{yy}. The experimental identification of these structures would be cogent proof for the long sought-after experimental discovery of a three-dimensional QSL.

Model.—In this analysis, we examine the *XYZ* model in the experimentally relevant octupolar dominant regime where $J_{yy} > 0$ and $J_{yy} > |J_{xx}|, |J_{zz}|$. In the Ising limit (i.e., $J_{yy} > 0$ and $J_{yy} \gg |J_{xx}|, |J_{zz}|$), the dominant term restricts the system to a subspace where the sum over the y component of all spins is zero for every tetrahedron (i.e., 2-in-2-out). The transverse couplings lead to mixing between these states and promote the system from a classical spin liquid to a QSL whose low-energy behavior

can be described by a compact $U(1)$ gauge theory of the form $\mathcal{H}_{\text{eff}} \sim (J_{xx} + J_{zz})^3/J_{yy}^2 \sum_\bigcirc \cos(\nabla \times \bar{A})$ on the parent diamond lattice [27,37,48,49]. From this perturbative argument, one expects a deconfined $U(1)$ QSL with 0 flux (π flux) threading the hexagonal plaquettes for $J_{xx} + J_{zz} < 0$ ($J_{xx} + J_{zz} > 0$). The stability of the 0-flux state is now firmly established from quantum Monte Carlo (QMC) simulations [46,47,50,51].

To go beyond such a perturbative treatment, we employ GMFT where a bosonic matter field that conceptually corresponds to tetrahedra breaking the 2-in-2-out rule is introduced on the parent diamond lattice [36,37,52–54]. In such a framework, the pseudospins are expressed in terms of an emergent compact $U(1)$ gauge field A, its canonically conjugate electric field E that takes on half-integer values, and the spinon operator $\Phi_{\mathbf{r}_\alpha}^\dagger = e^{i\varphi_{\mathbf{r}_\alpha}}$ that creates a gauge charge $Q_{\mathbf{r}_\alpha}$. Explicitly, $S_{\mathbf{r}_A + \mathbf{b}_\mu/2}^+ = \Phi_{\mathbf{r}_A}^\dagger (e^{iA_{\mathbf{r}_A, \mathbf{r}_A + \mathbf{b}_\mu}}/2)\Phi_{\mathbf{r}_A + \mathbf{b}_\mu}$ and $S_{\mathbf{r}_\alpha + \eta_\alpha \mathbf{b}_\mu/2}^y = \eta_\alpha E_{\mathbf{r}_\alpha, \mathbf{r}_\alpha + \eta_\alpha \mathbf{b}_\mu}$, where $S^\pm = S^z \pm iS^x$, $\mathbf{r}_\alpha$ labels the positions on the diamond lattice, $\eta_\alpha = 1(-1)$ if the site belongs to the $\alpha = A(B)$ sublattice, and $\mathbf{b}_\mu$ ($\mu = 0,1,2,3$) are vectors connecting the center of a tetrahedron to its four nearest-neighbor diamond lattice sites (see Supplemental Material [55] for conventions). Such a mapping is exact if the discretized Gauss's law $Q_{\mathbf{r}_\alpha} = \sum_{\mu=0}^3 E_{\mathbf{r}_\alpha, \mathbf{r}_\alpha + \eta_\alpha \mathbf{b}_\mu}$ is imposed on every tetrahedron.

Directly replacing the parton construction in the *XYZ* Hamiltonian leads to an interacting quantum rotor model strongly coupled to a compact $U(1)$ gauge field. To get a tractable model, three successive approximations are carried out. (i) A mean-field (MF) decoupling is performed on the four bosons interaction arising from terms of the form $S^\pm S^\pm$ such that $\Phi_i^\dagger \Phi_i^\dagger \Phi_j \Phi_k \to \Phi_i^\dagger \Phi_i^\dagger \chi_{j,k} + \Phi_j \Phi_k \bar{\chi}_{i,i}^0 + 2\Phi_i^\dagger \Phi_j \xi_{i,k} + 2\Phi_i^\dagger \Phi_k \xi_{i,j}$, where the intersite pairing χ, on-site pairing χ^0, and intersublattice hopping ξ MF parameters have been introduced. (ii) The gauge field is fixed to a constant saddle point background $A \to \bar{A}$. This effectively decouples the matter and dynamical gauge field sectors. (iii) Finally, a large-N approximation is made by relaxing the constraint on the rotor length $|\Phi_{\mathbf{r}_\alpha}^\dagger \Phi_{\mathbf{r}_\alpha}| = 1$ to an average one $\sum_{\mathbf{r}_\alpha} \langle \Phi_{\mathbf{r}_\alpha}^\dagger \Phi_{\mathbf{r}_\alpha} \rangle / N = \kappa$ for $\alpha = A, B$ imposed by the Lagrange multipliers λ^α. We pick $\kappa = 2$ since such a constraint recovers the correct spinon dispersion $\mathcal{E}_\gamma(\mathbf{k}) = J_{yy}/2$ in the Ising limit (i.e., $J_{xx}/J_{yy} \to 0$ and $J_{zz}/J_{yy} \to 0$). It also reproduces the QMC results for the position of the phase transition from the 0-flux QSI to an ordered state and for the position of the lower and upper edges of the two-spinon continuum [42,46,50]. See Supplemental Material [55] for detailed discussion, which includes Refs. [56–60]. Following these prescriptions, we get the GMFT Hamiltonian

$$\mathcal{H}_{\text{GMFT}} = \frac{J_{yy}}{2}\sum_{\mathbf{r}_\alpha} Q^2_{\mathbf{r}_\alpha} + \sum_{\mathbf{r}_\alpha}\lambda^\alpha(\Phi^\dagger_{\mathbf{r}_\alpha}\Phi_{\mathbf{r}_\alpha} - \kappa) - \frac{J_\pm}{4}\sum_{\mathbf{r}_\alpha}\sum_{\mu,\nu\neq\mu}\Phi^\dagger_{\mathbf{r}_\alpha+\eta_\alpha\mathbf{b}_\mu}\Phi_{\mathbf{r}_\alpha+\eta_\alpha\mathbf{b}_\nu}e^{i\eta_\alpha(\bar{A}_{\mathbf{r}_\alpha,\mathbf{r}_\alpha+\eta_\alpha\mathbf{b}_\nu}-\bar{A}_{\mathbf{r}_\alpha,\mathbf{r}_\alpha+\eta_\alpha\mathbf{b}_\mu})}$$

$$+\frac{J_{\pm\pm}}{8}\sum_{\mathbf{r}_\alpha}\sum_{\mu,\nu\neq\mu}\left[e^{i\eta_\alpha(\bar{A}_{\mathbf{r}_\alpha,\mathbf{r}_\alpha+\eta_\alpha\mathbf{b}_\nu}+\bar{A}_{\mathbf{r}_\alpha,\mathbf{r}_\alpha+\eta_\alpha\mathbf{b}_\mu})}(\Phi^\dagger_{\mathbf{r}_\alpha}\Phi^\dagger_{\mathbf{r}_\alpha}\chi_{\mathbf{r}_\alpha+\eta_\alpha\mathbf{b}_\mu,\mathbf{r}_\alpha+\eta_\alpha\mathbf{b}_\nu} + \bar{\chi}^0_{\mathbf{r}_\alpha,\mathbf{r}_\alpha}\Phi_{\mathbf{r}_\alpha+\eta_\alpha\mathbf{b}_\mu}\Phi_{\mathbf{r}_\alpha+\eta_\alpha\mathbf{b}_\nu}\right.$$

$$\left. + 2\Phi^\dagger_{\mathbf{r}_\alpha}\Phi_{\mathbf{r}_\alpha+\eta_\alpha\mathbf{b}_\mu}\xi_{\mathbf{r}_\alpha,\mathbf{r}_\alpha+\eta_\alpha\mathbf{b}_\nu} + 2\Phi^\dagger_{\mathbf{r}_\alpha}\Phi_{\mathbf{r}_\alpha+\eta_\alpha\mathbf{b}_\nu}\xi_{\mathbf{r}_\alpha,\mathbf{r}_\alpha+\eta_\alpha\mathbf{b}_\mu}) + \text{H.c.}\right], \tag{1}$$

where $J_\pm = -(J_{xx} + J_{zz})/4$ and $J_{\pm\pm} = (J_{zz} - J_{xx})/4$. A detailed construction of $\mathcal{H}_{\text{GMFT}}$ is presented in the Supplemental Material [55].

Phase diagram.—At this stage, one usually has to make an educated guess on the general form of the background gauge field and the other MF parameters [36,52,53]. Using a framework recently introduced by the authors [42], we make no such *ad hoc* assumptions and classify all field configurations that yield QSI states symmetric under all space group operations of the diamond lattice. The nontrivial transformation properties of the DO pseudospin moments lead to a distinct classification than in the effective spin-1/2 case [42]. For a chosen subset of inequivalent field configuration, we solve the self-consistency conditions and compute the ground state energy over the whole quadrupolar dominant quadrant to obtain the GMFT phase diagram presented in Fig. 1(c) (see Supplemental Material [55] for the classification).

The GMFT phase diagram is consistent with previous works [43,44]. We observe a large region where the spinon dispersion becomes gapless at the Γ point, thus leading to condensation of the bosons $\langle\Phi_{\mathbf{k}_c=\mathbf{0}}\rangle \neq 0$. This region corresponds to X or Z all-in-all-out magnetic ordering, as expected by classical simulations, since it has ordering wave vector $\mathbf{k}_c = \mathbf{0}$ and condensation implies $\langle S^\pm\rangle \sim e^{i\bar{A}}\langle\Phi^\dagger\rangle\langle\Phi\rangle \neq 0$.

Most significantly, we find the 0-O-QSI and π-O-QSI phases separated by the transition line $J_\pm = 0$, as predicted by the perturbative argument outlined above. Along the *XXZ* line (i.e., $J_{\pm\pm} = 0$), we find a transition from 0-O-QSI to the ordered state at $J_\pm/J_{yy} \approx 0.048$, in spectacular agreement with QMC where the transition occurs at $J_\pm/J_{yy} \approx 0.05$ [45–47,61]. In these deconfined QSI phases, the spinon spectrum is gapped, and all MF parameters vanish (i.e., $\chi = \chi^0 = \xi = 0$). When examining the GMFT Hamiltonian in Eq. (1), we see that the disappearance of the MF terms implies that the $U(1)$ symmetry breaking term associated with the $J_{\pm\pm}$ coupling vanishes as well. Even though this emergent $U(1)$ symmetry within the QSI phases might *a priori* seem like an artifact of GMFT, recent exact diagonalization (ED) results corroborate its naturalness [22]. ED calculations observed that for an anisotropic *XYZ* model (i.e., $J_{xx} \neq J_{yy} \neq J_{zz}$) in a parameter regime where the π-O-QSI should be stable, the equal-time pseudospin

correlations in the local frame [i.e., $\mathcal{S}^{ab}_{\text{LF}}(\mathbf{q}) = (1/N) \times \sum_{i,j}e^{-i\mathbf{q}\cdot(\mathbf{R}_i-\mathbf{R}_j)}\langle S^a_i S^b_j\rangle$] satisfy $\mathcal{S}^{xx}_{\text{LF}} = \mathcal{S}^{zz}_{\text{LF}}$, whereas in classical simulations $\mathcal{S}^{xx}_{\text{LF}} \neq \mathcal{S}^{zz}_{\text{LF}}$.

Equal-time correlations.—Now that the range of stability of 0-O-QSI and π-O-QSI has been established, we study their physical properties in detail. Since the S^x and S^y components of the pseudospins are octupolar in nature, they are not expected to linearly couple to the magnetic dipoles of neutrons. Accordingly, we assume that the only nonvanishing g factor in the local frame is g_{zz}, an accurate approximation for $Ce_2Zr_2O_7$ [18,19]. With $g_{xx} = g_{yy} = 0$, neutron scattering probes correlations between the local z components of the pseudospins associated with the spinon excitations ($S^z \sim \Phi^\dagger e^{i\bar{A}}\Phi$), not the photons ($S^y \sim E$).

We start by considering the equal-time correlations in both deconfined phases. On top of the diagonal equal-time pseudospin correlations $\mathcal{S}^{aa}_{\text{LF}}$, we compute the equal-time neutron scattering structure factor

$$\mathcal{S}(\mathbf{q}) = \frac{1}{N}\sum_{i,j}\left[\hat{z}_i\cdot\hat{z}_j - \frac{(\hat{z}_i\cdot\mathbf{q})(\hat{z}_j\cdot\mathbf{q})}{q^2}\right]e^{-i\mathbf{q}\cdot(\mathbf{R}_i-\mathbf{R}_j)}\langle S^z_i S^z_j\rangle, \tag{2}$$

where $\hat{z}_i$ is the local z axis at site i. With polarized neutrons, this total contribution can be separated into the spin-flip (SF) $\mathcal{S}_{\text{SF}}(\mathbf{q})$, and non-spin-flip (NSF) $\mathcal{S}_{\text{NSF}}(\mathbf{q})$ channels (neutrons are polarized perpendicular to the scattering plane). These results are presented in Fig. 2 for 0-O-QSI and π-O-QSI along the $[hhl]$ plane. The qualitative features of $\mathcal{S}_{\text{SF}}(\mathbf{q})$ are similar to $\mathcal{S}(\mathbf{q})$. Thus, we do not present $\mathcal{S}_{\text{SF}}(\mathbf{q})$ separately.

It should first be noted by looking at the equal-time correlations in the local frame and $\mathcal{S}(\mathbf{q})$ that the intensity gets reversed at the transition between 0-O-QSI and π-O-QSI while the pattern remains similar. This can be understood by considering the Ising limit where the ground state is an equal weight superposition of 2-in-2-out configurations in the y basis. Such a state corresponds to an equal weight superposition of all single tetrahedra configurations (i.e., 2-in-2-out, 3-in-1-out, 1-in-3-out, and all-in-all-out) in the x or z basis, leading to completely flat $\mathcal{S}^{xx}_{\text{LF}}(\mathbf{q})$, $\mathcal{S}^{zz}_{\text{LF}}(\mathbf{q})$, and $\mathcal{S}(\mathbf{q})$. Then in the 0-O-QSI (π-O-QSI) phase close to the Ising limit, the ferromagnetic (antiferromagnetic) transverse coupling favors the all-in-all-out (2-in-2-out) configurations. As argued in Ref. [62], decoupled
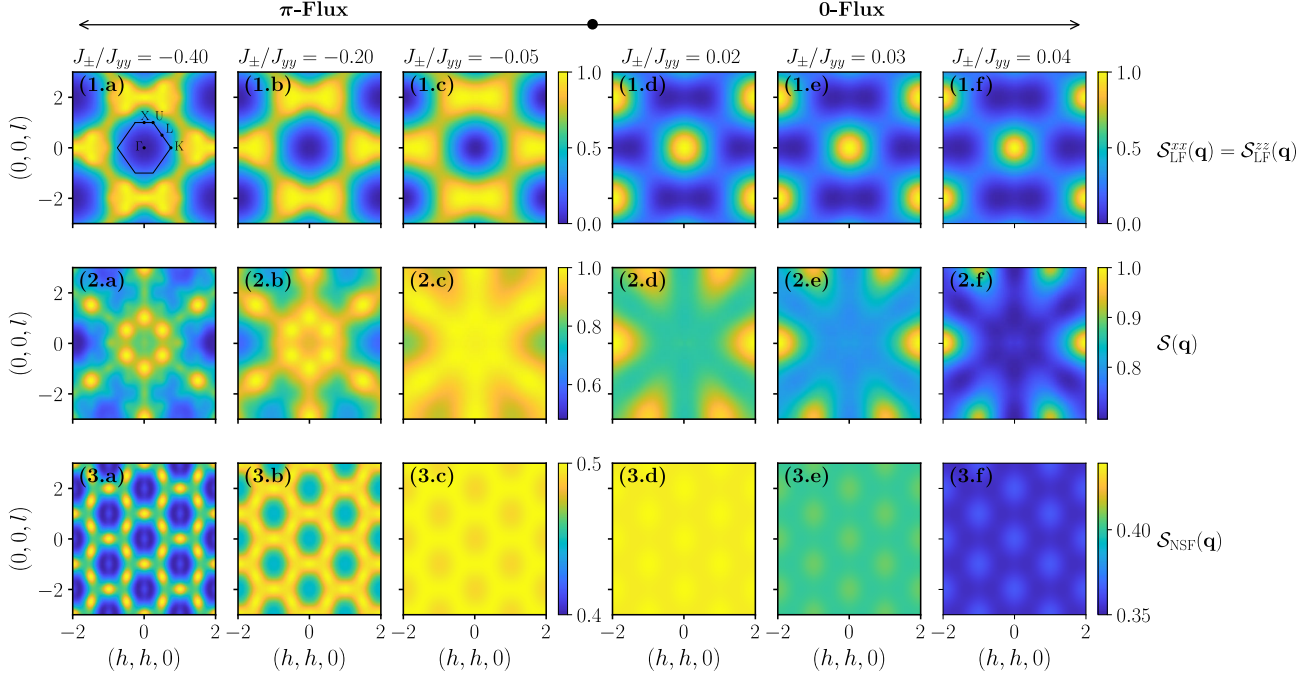
FIG. 2.   (top-1) Diagonal equal-time pseudospin correlations in the local frame for the transverse components, (middle-2) total neutron scattering equal-time structure factor and its contribution to the (bottom-3) non-spin-flip channel in the $[hhl]$ plane for π-O-QSI with $J_\pm/J_{yy}$ equal to (a) -0.40, (b) -0.20, and (c) -0.05 and 0-O-QSI with $J_\pm/J_{yy}$ equal to (d) 0.02, (e) 0.03, and (e) 0.04.

tetrahedra where all-in-all-out (2-in-2-out) configurations are favored lead to $\mathcal{S}(\mathbf{q})$ with flat high-intensity (low-intensity) rod motifs as observed in panel (2.c) (panel 2.d). Going further away from the Ising limit, the intensity of $\mathcal{S}_{\mathrm{LF}}^{xx}(\mathbf{q}) = \mathcal{S}_{\mathrm{LF}}^{zz}(\mathbf{q})$ keeps increasing at the (0,0,2) and (0,0,0) points for π-O-QSI and 0-O-QSI, respectively. The previous single-tetrahedron argument outlined above starts to fail, as signaled by an increasing intensity modulation along the rods in $\mathcal{S}(\mathbf{q})$. As correlations between tetrahedra in the z basis increase, we interestingly find a corresponding rise of the contrast in the NSF channels. This intensity modulation along the rods and in the NSF channels is especially striking considering that such features are observed in experiments and ED [15,18,22], but all classical calculations report completely flat rods and a featureless NSF channel [18,19,22]. Such features can only be obtained classically by artificially introducing next-nearest neighbor or dipolar interactions [19,63]. This observation seems to imply that the variations along the rods and in the NSF channel are due to quantum fluctuations that evade classical treatments. A detailed comparison presented in the Supplemental Material [55] shows that these equal-time correlations are consistent with the 32-site ED results of Ref. [22] and recent experimental measurements on $Ce_2Zr_2O_7$.

Dynamical correlations.—Next, we turn to the dynamical spin structure factor (DSSF). Figure 3 presents the spinon dispersion and DSSF between high symmetry points for 0-O-QSI and π-O-QSI. The intensity is concentrated near the upper edge of the two-spinon continuum for 0-O-QSI. A detailed analysis shows that predictions from GMFT are in excellent semiquantitative agreement with the QMC results of Ref. [50] for the 0-flux
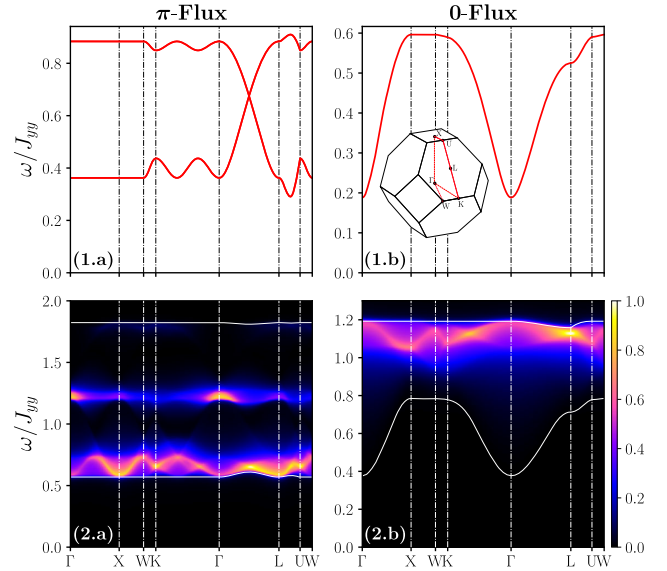

FIG. 3.   (top-1) Spinon dispersion and (bottom-2) dynamical spin structure factor for (a) π-O-QSI with $J_\pm/J_{yy} = -0.1875$ and (b) 0-O-QSI with $J_\pm/J_{yy} = 0.04$ along high-symmetry lines of the pyrochlore lattice first Brillouin zone. The solid white lines denote the upper and lower edges of the two-spinon continuum.
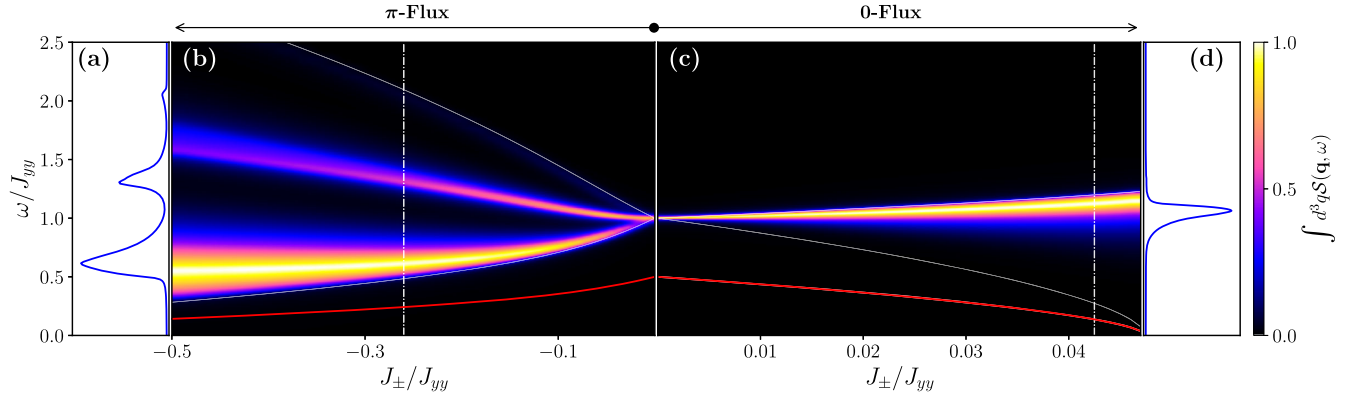
FIG. 4. Momentum-integrated dynamical spin structure factor for (b) π-O-QSI and (c) 0-O-QSI as a function of $J_{\pm}/J_{yy}$. Cuts at specific values of $J_{\pm}/J_{yy}$, indicated by the vertical white lines in (b) and (c), are presented in (a) and (d). The upper and lower edges of the two-spinon continuum are represented by solid white lines in (b) and (c), whereas the solid red lines indicate the spinon gap.

phase (see Supplemental Material [55]). We take this highly nontrivial check as convincing evidence that GMFT does provide a reliable description of spinons dynamics in QSI. In the case of π-O-QSI, the spinon dispersion is composed of two bands (the flux enlarges the unit cell [42,64]) that are mostly flat (i.e., standard deviation of the two bands is much lower than their separation). This leads to a two-spinon density $\rho^{(2)}(\omega) \sim \sum_{\alpha,\beta,\mathbf{q}_1,\mathbf{q}_2} \delta[\omega - \mathcal{E}_\alpha(\mathbf{q}_1) - \mathcal{E}_\beta(\mathbf{q}_2)]$ with three peaks coming from processes involving two spinons in the lowest band (lowest energy peak), the two different bands (central peak), and the highest band (highest energy peak) (see Supplemental Material [55] for further details). Since inelastic neutron scattering probes the two-spinon continuum, these three contributions are visible in the DSSF of π-O-QSI presented in panel (2.a) of Fig. 3, although the high energy peak close to the upper edges of the continuum is faint.

This continuum with three peaks is a distinctive signature. To see if it could still be measured by inelastic neutron scattering experiments on powder samples, we present the momentum-integrated DSSF as a function of $J_{\pm}/J_{yy}$ in Fig. 4. For $J_{\pm}/J_{yy} \to 0$, the DSSF collapses to a single peak at $\omega = J_{yy}$ since the spinon dispersion is entirely flat [i.e., $\mathcal{E}_\gamma(\mathbf{k}) = J_{yy}/2$] in that limit. A single peak concentrated near the upper edge of the two-spinon continuum is observed for 0-O-QSI from that point up to when the spinon gap vanishes and the bosons condense. For π-O-QSI, the three peaks are clearly discernible. As one moves from the Ising limit to the Heisenberg point, their separation as well as the relative intensity of the lowest energy peak compared to the second and third ones slowly increase. As a confirmation, we show in the Supplemental Material [55] that 32-site ED results display signatures of this multiple-peak structure despite strong finite-size limitations.

Discussion.—In this Letter, we used a newly introduced extension of GMFT to study octupolar QSI. We obtained a phase diagram consistent with previous studies where the deconfined 0-O-QSI and π-O-QSI phases are separated by the $J_{\pm} = 0$ line. We further showed that 0-O-QSI and π-O-QSI have energy-integrated neutron scattering signatures that have inverted intensities in momentum space and highlighted that GMFT produces the typical rod motifs observed in experiments with intensity modulation along the rods and in the NSF channels—features absent from classical treatments. It is then shown that 0-O-QSI has a DSSF with a single peak close to the upper edge of the two-spinon continuum, whereas π-O-QSI has three distinctive peaks resulting from two mostly flat spinon bands.

These three peaks provide a distinctive experimentally accessible smoking-gun signature for π-flux QSI. The third peak is most likely too faint to be measured, but high-resolution inelastic neutron scattering on powder samples should be able to observe the first two. For instance, using the microscopic parameters of Refs. [18,19], the separation of the first two peaks for $Ce_2Zr_2O_7$ should be approximately of 0.06 meV and could be resolved with the best available experimental apparatus [55].

Note added.—Recently, a new inelastic neutron scattering experiment on powder samples of material candidate $Ce_2Sn_2O_7$ achieved an energy resolution of 0.7 μeV and reported the presence of three peaks of decreasing intensity in the measured dynamical spin structure factor [65].

---

*felix.desrochers@mail.utoronto.ca
†ybkim@physics.utoronto.ca

[1] L. Savary and L. Balents, Rep. Prog. Phys. **80**, 016502 (2016).

[2] J. Knolle and R. Moessner, Annu. Rev. Condens. Matter Phys. **10**, 451 (2019).

[3] Y. Zhou, K. Kanoda, and T.-K. Ng, Rev. Mod. Phys. **89**, 025003 (2017).

[4] L. Balents, Nature (London) **464**, 199 (2010).

[5] C. Broholm, R. Cava, S. Kivelson, D. Nocera, M. Norman, and T. Senthil, Science **367**, eaay0668 (2020).

[6] X.-G. Wen, *Quantum Field Theory of Many-Body Systems: From the Origin of Sound to an Origin of Light and Electrons* (Oxford University Press on Demand, New York, 2004).

[7] X.-G. Wen, Phys. Rev. B **65**, 165113 (2002).

[8] X.-G. Wen, Rev. Mod. Phys. **89**, 041004 (2017).

[9] S. M. Winter, K. Riedl, P. A. Maksimov, A. L. Chernyshev, A. Honecker, and R. Valentí, Nat. Commun. **8**, 1 (2017).

[10] A. B. Harris, D. Kumar, B. I. Halperin, and P. C. Hohenberg, Phys. Rev. B **3**, 961 (1971).

[11] A. L. Chernyshev and M. E. Zhitomirsky, Phys. Rev. Lett. **97**, 207202 (2006).

[12] M. E. Zhitomirsky and A. L. Chernyshev, Rev. Mod. Phys. **85**, 219 (2013).

[13] A. Murani, J. Appl. Phys. **49**, 1604 (1978).

[14] S.-H. Lee, C. Broholm, G. Aeppli, A. Ramirez, T. Perring, C. Carlile, M. Adams, T. Jones, and B. Hessen, Europhys. Lett. **35**, 127 (1996).

[15] J. Gaudet, E. M. Smith, J. Dudemaine, J. Beare, C. R. C. Buhariwalla, N. P. Butch, M. B. Stone, A. I. Kolesnikov, G. Xu, D. R. Yahne, K. A. Ross, C. A. Marjerrison, J. D. Garrett, G. M. Luke, A. D. Bianchi, and B. D. Gaulin, Phys. Rev. Lett. **122**, 187201 (2019).

[16] B. Gao, T. Chen, D. W. Tam, C.-L. Huang, K. Sasmal, D. T. Adroja, F. Ye, H. Cao, G. Sala, M. B. Stone *et al.*, Nat. Phys. **15**, 1052 (2019).

[17] B. Gao, T. Chen, H. Yan, C. Duan, C.-L. Huang, X. P. Yao, F. Ye, C. Balz, J. R. Stewart, K. Nakajima, S. Ohira-Kawamura, G. Xu, X. Xu, S.-W. Cheong, E. Morosan, A. H. Nevidomskyy, G. Chen, and P. Dai, Phys. Rev. B **106**, 094425 (2022).

[18] E. M. Smith *et al.*, Phys. Rev. X **12**, 021015 (2022).

[19] A. Bhardwaj, S. Zhang, H. Yan, R. Moessner, A. H. Nevidomskyy, and H. J. Changlani, npj Quantum Mater. **7**, 1 (2022).

[20] E. Smith, O. Benton, D. Yahne, B. Placke, R. Schäfer, J. Gaudet, J. Dudemaine, A. Fitterman, J. Beare, A. Wildes *et al.*, Phys. Rev. X **14** 011005 (2023).

[21] F. Desrochers, L. E. Chern, and Y. B. Kim, Phys. Rev. B **105**, 035149 (2022).

[22] M. Hosoi, E. Z. Zhang, A. S. Patri, and Y. B. Kim, Phys. Rev. Lett. **129**, 097202 (2022).

[23] R. Sibille, E. Lhotel, V. Pomjakushin, C. Baines, T. Fennell, and M. Kenzelmann, Phys. Rev. Lett. **115**, 097202 (2015).

[24] R. Sibille, N. Gauthier, E. Lhotel, V. Porée, V. Pomjakushin, R. A. Ewings, T. G. Perring, J. Ollivier, A. Wildes, C. Ritter *et al.*, Nat. Phys. **16**, 546 (2020).

[25] V. Porée, E. Lhotel, S. Petit, A. Krajewska, P. Puphal, A. H. Clark, V. Pomjakushin, H. C. Walker, N. Gauthier, D. J. Gawryluk, and R. Sibille, Phys. Rev. Mater. **6**, 044406 (2022).

[26] V. Porée, A. Bhardwaj, E. Lhotel, S. Petit, N. Gauthier, H. Yan, V. Pomjakushin, J. Ollivier, J. A. Quilliam, A. H. Nevidomskyy *et al.*, arXiv:2305.08261.

[27] M. Hermele, M. P. A. Fisher, and L. Balents, Phys. Rev. B **69**, 064404 (2004).

[28] O. Benton, O. Sikora, and N. Shannon, Phys. Rev. B **86**, 075154 (2012).

[29] C. Castelnovo, R. Moessner, and S. L. Sondhi, Annu. Rev. Condens. Matter Phys. **3**, 35 (2012).

[30] C. Lacroix, P. Mendels, and F. Mila, *Introduction to Frustrated Magnetism: Materials, Experiments, Theory* (Springer Science & Business Media, New York, 2011), Vol. 164.

[31] M. Udagawa and L. Jaubert, *Spin Ice* (Springer, New York, 2021).

[32] J. G. Rau and M. J. Gingras, Annu. Rev. Condens. Matter Phys. **10**, 357 (2019).

[33] Y.-P. Huang, G. Chen, and M. Hermele, Phys. Rev. Lett. **112**, 167203 (2014).

[34] D. Yahne, B. Placke, R. Schäfer, O. Benton, R. Moessner, M. Powell, J. Kolis, C. Pasco, A. May, M. Frontzek *et al.*, arXiv:2211.15140.

[35] O. Benton, L. D. C. Jaubert, R. R. P. Singh, J. Oitmaa, and N. Shannon, Phys. Rev. Lett. **121**, 067201 (2018).

[36] S. B. Lee, S. Onoda, and L. Balents, Phys. Rev. B **86**, 104412 (2012).

[37] L. Savary and L. Balents, in *Spin Ice* (Springer, New York, 2021), pp. 239–271.

[38] M. Taillefumier, O. Benton, H. Yan, L. D. C. Jaubert, and N. Shannon, Phys. Rev. X **7**, 041057 (2017).

[39] Y.-D. Li and G. Chen, Phys. Rev. B **95**, 041106(R) (2017).

[40] X.-P. Yao, Y.-D. Li, and G. Chen, Phys. Rev. Res. **2**, 013334 (2020).

[41] G. Chen, Phys. Rev. B **96**, 085136 (2017).

[42] F. Desrochers, L. E. Chern, and Y. B. Kim, Phys. Rev. B **107**, 064404 (2023).

[43] A. S. Patri, M. Hosoi, and Y. B. Kim, Phys. Rev. Res. **2**, 023253 (2020).

[44] O. Benton, Phys. Rev. B **102**, 104408 (2020).

[45] N. Shannon, O. Sikora, F. Pollmann, K. Penc, and P. Fulde, Phys. Rev. Lett. **108**, 067204 (2012).

[46] C.-J. Huang, C. Liu, Z. Meng, Y. Yu, Y. Deng, and G. Chen, Phys. Rev. Res. **2**, 042022(R) (2020).

[47] A. Banerjee, S. V. Isakov, K. Damle, and Y. B. Kim, Phys. Rev. Lett. **100**, 047208 (2008).

[48] M. J. Gingras and P. A. McClarty, Rep. Prog. Phys. **77**, 056501 (2014).

[49] C. L. Henley, Annu. Rev. Condens. Matter Phys. **1**, 179 (2010).

[50] C.-J. Huang, Y. Deng, Y. Wan, and Z. Y. Meng, Phys. Rev. Lett. **120**, 167202 (2018).

[51] N. Shannon, in *Spin Ice* (Springer, New York, 2021), pp. 273–301.

[52] L. Savary and L. Balents, Phys. Rev. Lett. **108**, 037202 (2012).

[53] L. Savary and L. Balents, Phys. Rev. B **87**, 205130 (2013).

[54] Z. Hao, A. G. R. Day, and M. J. P. Gingras, Phys. Rev. B **90**, 214430 (2014).

[55] See Supplemental Material at http://link.aps.org/supplemental/10.1103/PhysRevLett.132.066502 for conventions used in the main text, the relationship between the *XYZ* Hamiltonian and the original dipolar-octupolar model, the classification of U(1) symmetric dipolar-octupolar spin liquids within gauge mean-field theory, details on how to evaluate observables for the different fractionalization classes, detailed comparison between the results from GMFT and numerical estimates of exact diagonalization and quantum Monte Carlo for equal-time and dynamical correlations, and predictions for the dynamical spin structure factor of candidate material cerium zirconate.

[56] F. Wang and A. Vishwanath, Phys. Rev. B **74**, 174423 (2006).

[57] L. Messio, C. Lhuillier, and G. Misguich, Phys. Rev. B **87**, 125127 (2013).

[58] S. Bieri, C. Lhuillier, and L. Messio, Phys. Rev. B **93**, 094437 (2016).

[59] S. Sachdev, Phys. Rev. B **45**, 12377 (1992).

[60] L. Messio, O. Cépas, and C. Lhuillier, Phys. Rev. B **81**, 064428 (2010).

[61] Y. Kato and S. Onoda, Phys. Rev. Lett. **115**, 077202 (2015).

[62] C. Castelnovo and R. Moessner, Phys. Rev. B **99**, 121102(R) (2019).

[63] K. T. K. Chung, J. S. K. Goh, A. Mukherjee, W. Jin, D. Lozano-Gómez, and M. J. P. Gingras, Phys. Rev. Lett. **128**, 107201 (2022).

[64] A. M. Essin and M. Hermele, Phys. Rev. B **90**, 121102(R) (2014).

[65] V. Porée, H. Yan, F. Desrochers, S. Petit, E. Lhotel, M. Appel, J. Ollivier, Y. B. Kim, A. H. Nevidomskyy, and R. Sibille, arXiv:2304.05452.